

Article

Deconstruction of high-density polyethylene into liquid hydrocarbon fuels and lubricants by hydrogenolysis over Ru catalyst



Plastic pollution has become one of the most pressing environmental issues and needs to be tackled imminently. Here, Lin and coworkers report a liquid-phase catalytic hydrogenolysis process that highly efficiently converts high-density polyethylene (PE) to jet-fuel- and lubricant-range hydrocarbons under relatively mild conditions. Solvents profoundly affect the depolymerization reaction kinetics and product selectivity. This work provides a promising approach for selectively producing high-value products, such as jet fuel and lubricants, from waste PE and other polyolefin polymers.

Chuhua Jia, Shaoqu Xie, Wanli Zhang, Nadia N. Intan, Janani Sampath, Jim Pfaendtner, Hongfei Lin

hongfei.lin@wsu.edu

Highlights

Ru/C was a highly active catalyst for the liquid-phase hydrogenolysis of HDPE

Solvent effects were prominent in the depolymerization of HDPE

H₂ partial pressure played a significant role in the HDPE depolymerization pathway

Total yield of liquid products reached around 90 wt % within 1 h at 220°C





Jia et al., Chem Catalysis 1, 437–455 July 15, 2021 © 2021 Elsevier Inc. https://doi.org/10.1016/j.checat.2021.04.002





Article

Deconstruction of high-density polyethylene into liquid hydrocarbon fuels and lubricants by hydrogenolysis over Ru catalyst

Chuhua Jia, ¹ Shaoqu Xie, ¹ Wanli Zhang, ¹ Nadia N. Intan, ² Janani Sampath, ³ Jim Pfaendtner, ^{2,3} and Hongfei Lin^{1,4,*}

SUMMARY

Polyethylene (PE) is the most popular plastic globally, and the widespread use of plastics has created severe environmental issues. High energy consumption in the current process makes its recycling a challenging problem. In our report, the depolymerization of high-density PE was conducted in various liquid-phase solvents with the Ru/C catalyst under relatively mild conditions. The maximum yields of the jet-fuel- and lubricant-range hydrocarbons were 60.8 and 31.6 wt %, respectively. After optimization of the reaction conditions (220°C and 60 bar of H₂), the total yield of liquid hydrocarbon products reached approximately 90 wt % within only 1 h. The product distribution could be tuned by the H₂ partial pressure, the active-metal particle size, and the solvents. The solvation of PE in the different solvents determined the depolymerization reaction kinetics, which was confirmed by the molecular dynamics simulation results.

INTRODUCTION

The accumulation of waste plastics in landfills and oceans has caused a global environmental crisis. 1-3 In particular, microplastics have been entering the food chain and become a potential threat to human health (B. Liebmann et al., 2018, Microplastics 2018, conference). Although there are thousands of plastic materials in use, only six of them—polyethylene (PE, high and low density), polypropylene, poly(vinyl chloride), polystyrene (including expanded polystyrene), polyurethane, and poly(ethylene terephthalate)—are widely used. Collectively, ~6.3 billion metric tons of plastic waste were produced by 2015, of which 79% was landfilled, 12% was incinerated, and only 9% was recycled. PE is the polymer with the most massive volume produced globally, and the production could reach over 100 million metric tons per year.^{4,5} Therefore, the efficient upcycling of waste plastics, especially PE, is critical to mitigating the severe environmental problem.

Technologies for recycling waste plastics mainly include three types: mechanical recycling, incineration, and chemical recycling. Mechanical recycling is the only technology used commercially for the large-scale plastic recycling process, but it still suffers from decreasing product quality after the consecutive melting and remolding cycles. 6 Although incineration converts mixed waste plastics to heat and electricity, the energy recovery efficiency cannot be as much as that from chemical recycling because of the massive loss of energy. Therefore, chemical recycling is considered a promising process for valorizing waste plastics, whereby plastics are the low-cost feedstock for producing value-added chemicals or fuels.

The bigger picture

Plastic pollution has become one of the most pressing environmental issues now that the rapidly increased production of disposable plastic products is far beyond the world's capacity for recycling and upcycling waste plastics. Although recent studies have provided a few catalytic strategies for producing valueadded fuel and chemical products from polyethylene (PE) waste, the kinetic rates and/or selectivities are unsatisfactory, even with extended processing time (24 h) and high temperatures (>280°C). This work reports a liquid-phase catalytic hydrogenolysis process that highly efficiently converts high-density PE to jet-fuel- and lubricant-range hydrocarbons under relatively mild conditions. The application of this efficient liquid-phase catalytic hydrogenolysis process could provide a promising approach for selectively producing high-value products, such as lubricants, from waste PE and other polyolefin polymers.





Chem Catalysis Article

Recently, pyrolysis has been extensively investigated as a chemical recycling technology. The world's largest resin producers, including Chevron Phillips Chemical (CPC), Saudi Basic Industries Corporation, and BASF, have been using this technology to produce circular polymers from plastic waste. B-10 Indeed, CPC has already accomplished the first commercial-scale production of circular PE in the United States. In addition to the commercial application, catalytic pyrolysis has also drawn much interest from research communities. The production of syngas or liquid hydrocarbon fuels from PE waste is technically feasible. However, elevated temperatures (>300°C) are needed in catalytic pyrolysis processes, which might not be economically sound given the high energy consumption. Moreover, it is challenging to control product distribution at high temperatures. In addition to linear alkanes, branched, cyclic, and aromatic hydrocarbons are produced during pyrolysis. F-17 Aromatics are of value, but they can readily be transformed into coke that might cause catalyst deactivation. E-21 Even though the catalyst could be regenerated after the coke is burned, the operation cost would increase substantially.

Therefore, developing effective catalytic processes that could selectively convert PE to high-value chemicals under mild reaction conditions is of utmost importance for chemical upcycling of PE waste plastics. ²² For instance, Sadow and coworkers ²³ designed a mesoporous catalyst with a Pt core@SiO₂ shell structure to selectively convert high-density PE (HDPE) into a narrow distribution of diesel- and lubricant-range alkanes in a solvent-free system (300°C, 24 h, 1.38 MPa H₂). The polymer molecules thread and bind into the silica pores, and the small-molecule products desorb and exit the pores after the cleavage from the polymer end at the active sites on the Pt metal catalyst surface. Likewise, Scott and coworkers ²⁴ developed a tandem solvent-free hydrogenolysis-aromatization process to produce valuable alkyl aromatics from PE with a Pt/Al₂O₃ catalyst at 280°C. Although these solvent-free methods provided a strategy for manufacturing higher-value products from PE waste, the kinetic performance is still an issue because it requires an extended processing time (24 h).

In general, compared with solvent-free pyrolysis, PE depolymerization can be promoted dramatically with the use of solvents, where mass transfer and heat transfer rates can be improved. PE at 120°C, and the yield of low-molecular-weight hydrocarbons reached 95% in 72 h. Although the reaction temperature was much lower, the reaction time had to be prolonged to achieve satisfactory outcomes. Meanwhile, the separation might be an issue given that another solvent was needed for extracting the products from the ionic liquid solvent. Jia et al. Pe was degraded into transportation fuels and waxes through cross-alkane metathesis with hexane, 98% of which were converted into liquid hydrocarbon oils at 150°C in 3 days. Ideally, a well-designed solvent system with appropriate heterogeneous catalysts could promote highly selective PE depolymerization under mild conditions. However, for the current solvolysis process, catalytic deconstruction rates still need to be enhanced. Practically, the recovery, reuse, and lifetime of solvents and catalysts could also be limiting factors for large-scale applications.

In our previous study, we found that ruthenium on a carbon (Ru/C) catalyst was able to convert *n*-heptadecane into short-chain hydrocarbons under mild conditions. The Ru catalyst is known to be capable of cleaving the C–C bond. ^{30,31} The dehydrogenative chemisorption of the hydrocarbons is considered the first step in the mechanism of hydrogenolysis on active metal, and then the formed hydrogen-deficient surface species go through C–C bond scission. ³² After the cleavage of C–C, the reaction is finally completed by hydrogenation and desorption. PE, consisting of

¹Gene and Linda Voiland School of Chemical Engineering and Bioengineering, Washington State University, Pullman, WA 99164, USA

²Department of Chemical Engineering, University of Washington, Seattle, WA 98195, USA

³Physical Sciences Division, Pacific Northwest National Laboratory, Richland, WA 99352, USA

Lead contact

^{*}Correspondence: hongfei.lin@wsu.edu https://doi.org/10.1016/j.checat.2021.04.002



Table 1. Physicochemical characterization results for the Ru/C catalysts							
Catalyst	S_{BET} (m ² g ⁻¹)	Particle size (nm)	Ru dispersion	Metallic surface area ($m^2 g^{-1}$)			
Fresh Ru/C	737.0	2.9	33.1%	8.1			
Ru/C-used cycle 1	704.3	4.1	24.3%	5.9			
Ru/C-used cycle 2	689.0	4 1	24.3%	5.9			

long hydrocarbon chains, has the simplest structure of any of the polymers. While our manuscript was under review, the remarkably high activity of the Ru catalyst in the hydrogenolysis of PE was also reported by Rorrer et al. in the absence of solvent. We hypothesize that Ru catalysts can break the C–C bonds in PE polymers by using a suitable solvent. Hence, in the current study, we investigated the conversion of PE to liquid fuels with a Ru/C catalyst in the liquid-phase reaction, which has not been reported previously to the best of our knowledge.

RESULTS

Characterization of catalysts

Table 1 shows the structural parameters of fresh and spent Ru/C catalysts. The specific surface area, the metallic surface area, and the active-metal dispersion decreased after the first run but remained the same after the second run. The result showed that the catalyst structure became stable after the first cycle. The decrease in Ru dispersion could be partly due to metal leaching during the reaction. The Ru particle size increased from 2.9 to 4.1 nm, indicating that sintering occurred after the first run. These structural changes could explain the decrease in the catalytic activity after the first run.

Transmission electron microscopy (TEM) images of the fresh and spent Ru/C catalysts are displayed in Figure 1, showing that the Ru nanoparticles were well dispersed on the C support. The mean particle size on the fresh catalyst was approximately 3.1 nm. A slight shift in the particle-size distribution was observed on the used catalysts, although the particle size was in the range of 2–5 nm. According to the TEM images, the mean particle size of the spent Ru/C catalysts after the first and second cycles was 4.2 and 4.0 nm, respectively, which is consistent with the CO pulse chemisorption result. Both characterization results demonstrated that the aggregation occurred on the Ru/C catalyst after the first cycle, whereas the Ru particle size was nearly unchanged in the subsequent cycles.

We employed X-ray photoelectron spectroscopy (XPS) to investigate the change in valence state in the Ru particles before and after the reaction. Because the Ru 3d doublet overlaps C 1s, Ru 3p is commonly used for characterizing the change in the Ru element valence state. Figure 2 shows that the Ru $3p_{1/2}$ and $3p_{3/2}$ binding energies of the fresh Ru/C catalyst were 462.9 and 485.0 eV, respectively, whereas those of the spent catalyst shifted to low values, 462.4 and 484.8 eV, respectively, after the reaction, indicating that Ru oxide on the catalyst was reduced by H_2 during the reaction. Meanwhile, the Ru atomic percentage decreased from 1.6% to 1.05% after the first cycle, whereas it remained the same after the second cycle, which is consistent with the trend of the decrease in the metallic surface area in Table 1.

The crystalline structures of the fresh and used catalysts before and after the HDPE depolymerization, respectively, were characterized through X-ray diffraction (XRD) (Figure 3). Two XRD peaks at about $2\theta = 25^{\circ}$ and 43° are associated with the (002) and (100) phases of the C support, respectively. No Ru or Ru oxide peaks were



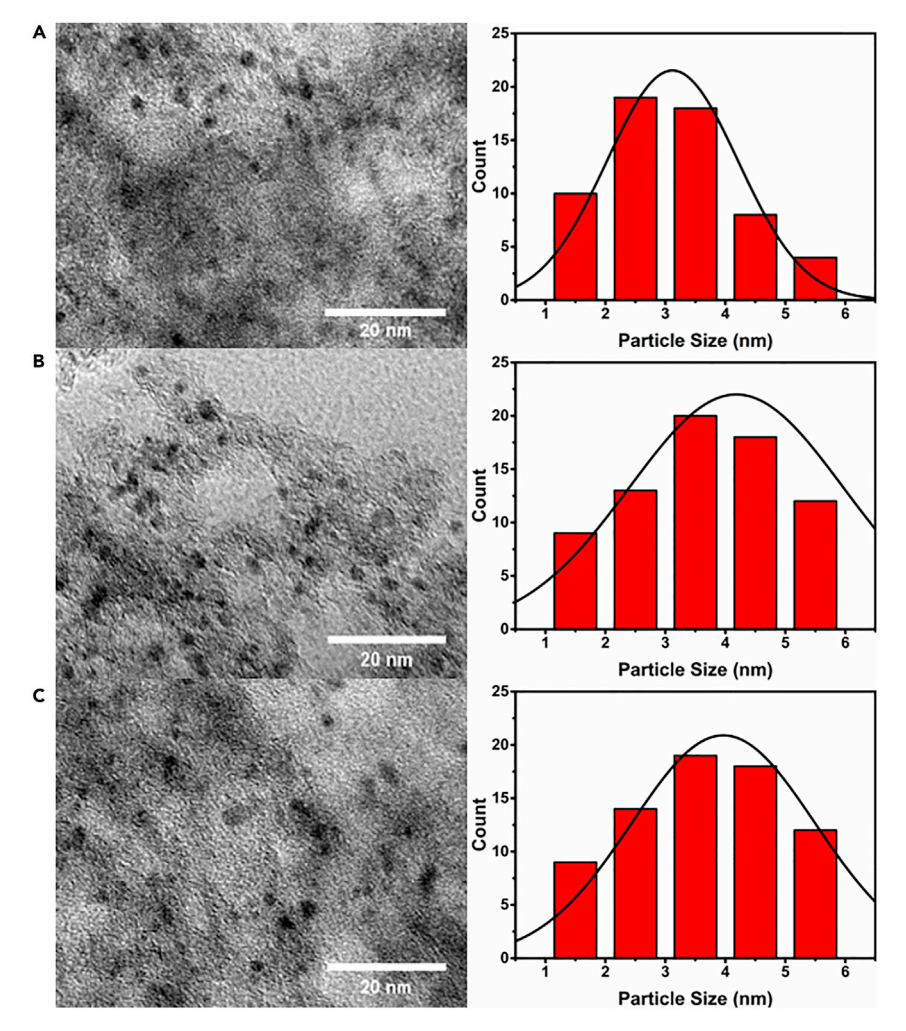


Figure 1. Fresh and spent Ru/C catalysts

TEM images and particle-size-distribution histograms of (A) Ru/C fresh, (B) Ru/C used cycle 1, and (C) Ru/C used cycle 2. Reaction conditions: 0.1 g HDPE, 0.05 g Ru/C, 25 mL n-hexane, 220°C, p(H₂) 20 bar, 1 h, 700 rpm.

observed, indicating that the Ru particles were very small and dispersed on the C support very well. 34 No significant change in the XRD patterns was observed before or after the reaction, implying that the catalyst's crystal structure might be unchanged.

Catalyst screening

The HDPE depolymerization reaction was investigated with a variety of C-supported metal catalysts under the same reaction conditions. The experimental results in Table 2 show that the copper, iron, palladium, platinum, and nickel catalysts displayed no effect on the HDPE depolymerization at 220°C. Although other groups have reported that iron, palladium, and nickel can promote PE deconstruction, high temperatures (e.g., 430°C) are still necessary for such processes. 35,36 Recently, Pt@SiO2 catalysts were reported to carry out the hydrogenolysis of HDPE in a solvent-free system for an extended reaction time, 24 h, at a relatively low temperature (250°C). 23 In contrast, in our study, only <0.5 wt % of the HDPE depolymerization products (C8–C38) was detected on gas chromatography-mass spectrometry

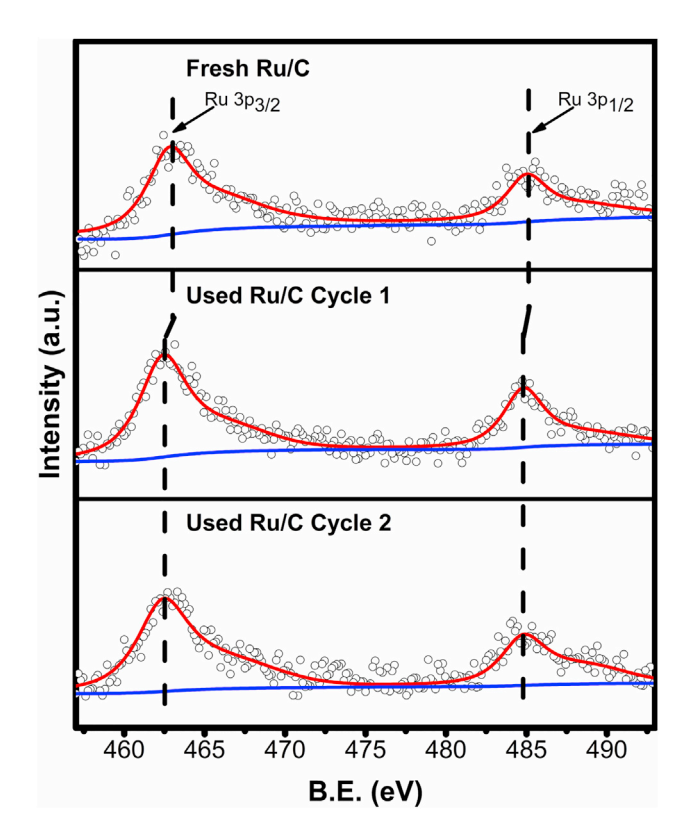


Figure 2. XPS spectra of fresh and spent Ru/C Reaction conditions: 0.1 g HDPE, 0.05 g Ru/C, 25 mL n-hexane, 220°C, p(H₂) 20 bar, 1 h, 700 rpm. B.E., binding energy.

(GC-MS) with the Pt/C catalyst in n-hexane even when it was reacted for 6 h at 250°C. The solvent system's poor performance could be ascribed to HDPE's low solubility in supercritical n-hexane (critical temperature: 234.5°C). Rhodium (Rh) was reported to have catalytic ability in C-C cracking, which is similar to Ru. ³⁷ However, with the Rh/C catalyst, no detectable liquid hydrocarbon products by GC-MS were observed at 220°C, although there was no residue after the reaction. Long-chain hydrocarbons (>C45) with high molecular weights, which are beyond the detection limit of our mass spectrometer, could be the main products. As the temperature increased to 280°C, an ~75.3 wt % yield of alkanes in the range of C8-C38 was obtained (Figure S1A), demonstrating that Rh is also active for C-C hydrogenolysis at elevated temperatures. In contrast, the full conversion of HDPE to hydrocarbon fuels by pyrolysis with the Ru/Y-zeolite catalyst was accomplished at 600°C. However, the severe coke deposition on the catalyst in pyrolysis raised concerns about the catalyst's stability.³⁸ Here, we found that the Ru/C catalyst was superior among all the screened catalysts in this study. The HDPE strips were converted to 60.8 wt % jet-fuel-range and 14.1 wt % diesel-range alkanes at 220°C in just 1 h with the Ru/C catalyst in nhexane, and no long-chain products could be detected (Figure S1B). Compared with other metals, Ru metal was reported to have the lowest activation energy in ethane hydrogenolysis, favoring the C-C bond cleavage. 32 In the comparison of ethane hydrogenolysis on transition-metal catalysts, *CHCH* was found to be the primary intermediate in the C-C bond scission for Ru, Rh, and Pt because it has the lowest free-energy barrier in C-C bond cleavage.³⁹ Meanwhile, both *CHCH* and *CH3CH* were considered dominant intermediates for Pd. Among these transition metals, the turnover rate in *CHCH* cleavage decreases in the order



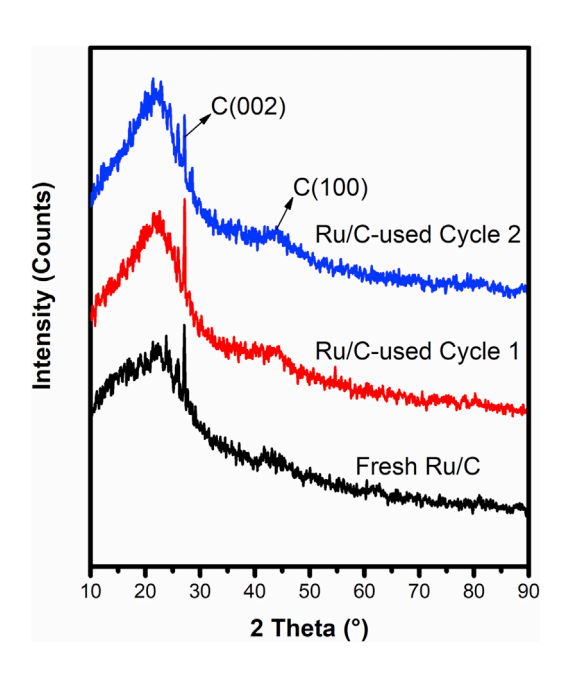


Figure 3. Powder XRD patterns of the fresh and spent Ru/C catalysts Reaction conditions: 0.1 g HDPE, 0.05 g Ru/C, 25 mL n-hexane, 220°C, p(H₂) 20 bar, 1 h, 700 rpm.

Ru > Rh > Pt > Pd, which is consistent with our result that Ru could cleave the C-C efficiently and that Pd has the lowest cleavage turnover rate.

Tuning reaction parameters

The temperature effect on the HPDE depolymerization is shown in Figure 4A. We detected no cracking product at 150°C. When the depolymerization was carried out at 200°C, a complete HDPE conversion to liquid-phase alkanes was obtained. With increasing temperature, the yield of high-molecular-weight alkane products decreased. The yield of the jet-fuel-range alkanes (C8-C16) reached a maximum of ~60 wt %, whereas that of the diesel fuels (C17-C22) was ~15 wt % at 220°C, and almost all long-chain hydrocarbons (C number > 23) were converted to shortchain alkanes in 1 h. As the temperature increased to 230°C, the yields of jet- and diesel-fuel-range alkanes decreased to ~55 and ~5 wt %, respectively, as a result of excess cracking. The HDPE polymer is not easily solvated in a supercritical solvent. At 240°C, which is higher than n-hexane's critical temperature (234.5°C), we observed an abrupt change in the product distribution compared with that at

Entry	Feedstock	Catalyst	Temperature (°C)	Time (h)	C8-C16 (wt %)	C17-C22 (wt %)	C23-C38 (wt %)
1	HDPE	5% Cu/C	220	1	0	0	0
2	HDPE	5% Fe/C	220	1	0	0	0
3	HDPE	5% Ni/C	220	1	0	0	0
4	HDPE	5% Pt/C	220	1	0	0	0
5	HDPE	5% Pd/C	220	1	0	0	0
6	HDPE	5% Rh/C	220	1	0	0	0
7	HDPE	5% Ru/C	220	1	60.8	14.1	0
8	HDPE	5% Pt/C	250	6	0.2	0.16	0.23
9	HDPE	5% Pd/C	280	1	0.29	0.01	0.1
10	HDPE	5% Pt/C	280	1	0.28	0.37	0.42
11	HDPE	5% Rh/C	280	1	21.7	20.2	33.4



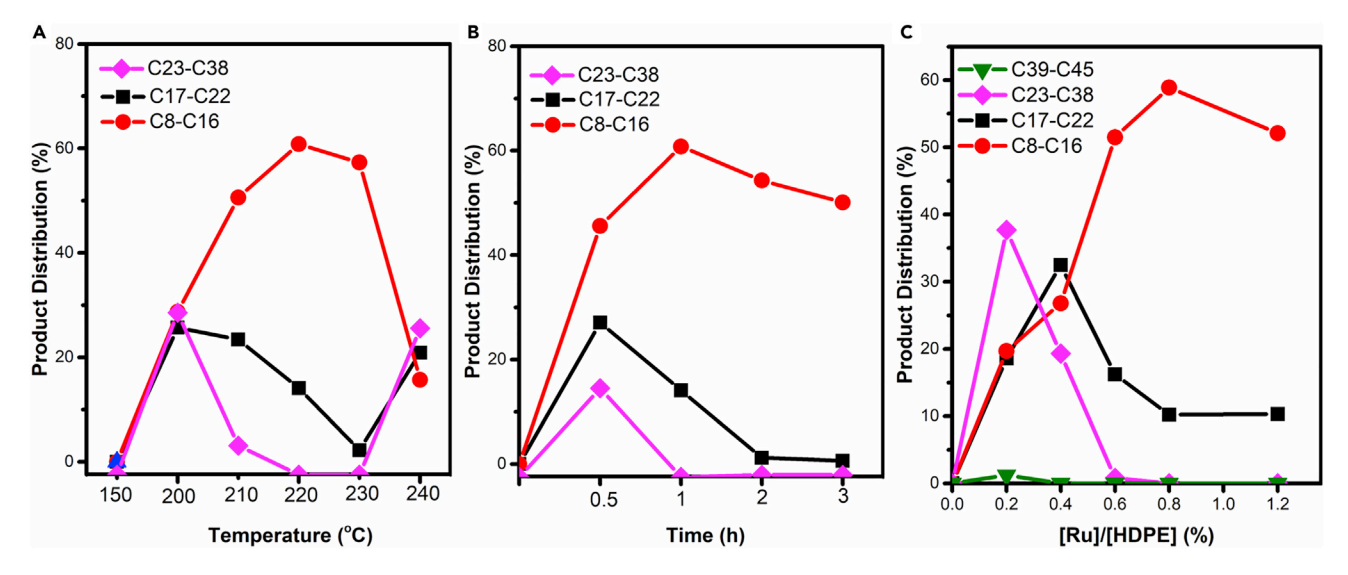


Figure 4. Temperature, reaction time, and catalyst loading effect

(A) Temperature profile of the production distribution of the HDPE depolymerization. Reaction conditions: 0.1 g HDPE, 0.05 g Ru/C, 25 mL n-hexane, p(H₂) 30 bar, 1 h, 700 rpm.

(B) Reaction-time profile of the production distribution of the HDPE depolymerization. Reaction conditions: 0.1 g HDPE, 0.05 g Ru/C, 25 mL n-hexane, 220°C, $p(H_2)$ 30 bar, 700 rpm.

(C) Catalyst loading effect on the production distribution of the HDPE depolymerization. Reaction conditions: 0.1 g HDPE, 25 mL n-hexane, 220°C, p(H₂) 20 bar, 1 h, 700 rpm. The effective catalyst loading M_{Ru}/M_{HDPE} wt % was calculated as follows: M_{Ru}/M_{HDPE} wt % = ([mass of the Ru/C catalyst] \times [5 wt %] \times [Ru dispersion])/(mass of HDPE strips). The remaining products are short-chain hydrocarbons (C1–C7).

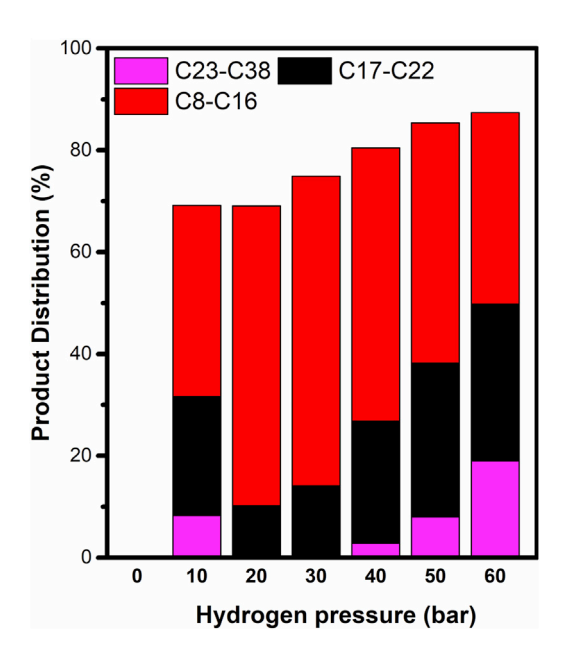
230°C. The yield of the long-chain hydrocarbon products (C17–C38) increased dramatically from <5 to \sim 50 wt % as the temperature increased just 10°C (from 230°C to 240°C), implying that the low solubility of HDPE in the supercritical *n*-hexane solvent could lead to much slower C–C bond cracking rates.

The reaction time is another crucial parameter for determining the product distribution. Here, the effect of reaction time on the HDPE depolymerization was also investigated, and the results are shown in Figure 4B. Surprisingly, HDPE was rapidly degraded to liquid hydrocarbons (C number < 38) in only 0.5 h at 220°C. With increasing reaction time, the yield of jet-fuel-range alkanes increased first and then decreased as a result of excess cracking. The maximum yield (~60 wt %) of jet-fuel-range alkanes was achieved in 1 h. Almost no high-molecular-weight products were observed after 1 h.

Further, we also investigated the catalyst loading effect on the depolymerization by varying the amount of catalyst. As shown in Figure 4C, the depolymerization reaction did not occur in the absence of a catalyst. The depolymerization reaction rate increased with increasing catalyst loading. With a low loading of the catalyst ([Ru]/ [HDPE] ratio was 2.1%), the yield of lubricant-range hydrocarbons (C24–C35) reached 31.6%. While the [Ru]/[HDPE] ratio increased to 8.3%, the yield of jetfuel-range alkanes achieved the maximum value (\sim 60 wt %). As the catalyst amount continued to increase, the corresponding jet-fuel yield decreased. Meanwhile, more short-chain hydrocarbons (C number < 8) were observed after the [Ru]/[HDPE] ratio surpassed 1.2%, indicating that an increasing amount of catalyst would promote the cracking reaction.

Figure 5 shows that hydrogen pressure played a significant role in the HDPE depolymerization. In the absence of H_2 , no product was detected. With increasing H_2





HDPE
Reaction conditions: 0.1 g HDPE,
0.05 g Ru/C, 25 mL *n*-hexane,
220°C, 1 h, 700 rpm. The remaining
products are short-chain
hydrocarbons (C1–C7).

Figure 5. Hydrogen pressure

effect on depolymerization of

pressure from 0 to 60 bar, the depolymerization reaction rate increased first and then decreased after the H₂ pressure passed 30 bar, indicating that higher hydrogen pressure could inhibit the depolymerization reaction. Iglesia and coworkers also observed that hydrogenolysis of the linear and branched alkanes (C2-C8) was reduced as the H₂ pressure increased. 40 They found that H₂ pressure could also influence the C-C bond cleavage position in long-chain alkanes, probably as a result of the dehydrogenated intermediates formed by quasi-equilibrated adsorption and dehydrogenation. 41,42 At low hydrogen pressures, the hydrogenolysis rates were proportional to the concentration of the reactive unsaturated intermediate $[^*C_nH_{2n+2-v}^*]$, and the rates increased with hydrogen pressure. ⁴³ At high hydrogen pressures, the surface was mainly occupied by chemisorbed hydrogen atoms (H*), hindering the adsorption of intermediates and decreasing the hydrogenolysis rates. Note that Iglesia and coworkers studied the alkane hydrogenolysis in the gas phase, which could significantly differ from PE's hydrogenolysis in solvents. HDPE's structure resembles those of long-C-chain linear alkanes (varying in C chain length), consisting of only $C_{secondary}$ - $C_{primary}$ and $C_{secondary}$ - $C_{secondary}$ bonds. Hence, the Ru-catalyzed HDPE hydrogenolysis includes primarily two independent reactions: regioselective hydrogenolysis of the easily accessible C-C bonds (e.g., $C_{secondary}$ - $C_{secondary}$) and hydrogenolysis of $C_{secondary}$ - $C_{primary}$ bonds (i.e., chainend scission). 44 Thus, the scission of $C_{secondary}$ – $C_{secondary}$ is preferred for acquiring more valuable long-chain hydrocarbons.

Also, the hydrogenolysis mechanism of linear liquid-phase alkanes would be analogous to the dissociation mechanism for the C–C bonds in HDPE and its degradation intermediates. Herein, the hydrogen pressure effect was further explored with eicosane, a C20 linear alkane, as the probe reactant (Figure 6). We found that at low $\rm H_2$ pressure (10 bar), the C19 alkane, n-nonadecane, was the dominant product, indicating that terminal dissociation was the main pathway. As the $\rm H_2$ pressure increased to 60 bar, the main products were octadecane and heptadecane ($\rm C_{18}H_{38}$ and $\rm C_{17}H_{36}$), demonstrating that the primary pathway was changed to internal dissociation. Nakagawa et al. reported that with a $\rm Ru/CeO_2$ catalyst and the absence of solvents, the reaction order to the $\rm H_2$ partial pressure for cracking n-hexadecane ($\rm C_{16}H_{34}$) was 0.4. Non-stoichiometric methane formation from n-hexadecane

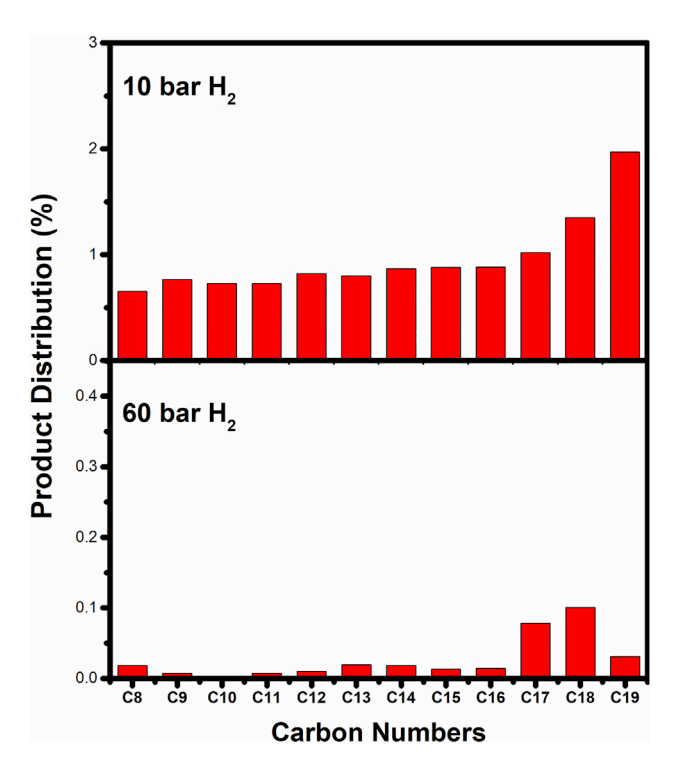


Figure 6. The liquid alkane product (C_8 – C_{19}) distribution from eicosane hydrogenolysis over the Ru/C catalyst

Reaction conditions: 0.1 g eicosane, 0.05 g Ru/C, 25 mL n-hexane, 200°C, 0.3 h. The remaining products are short-chain hydrocarbons (C1–C7).

([methane] - [C_{15}] = -0.8) was observed, indicating that high hydrogen pressure suppressed excess methane formation, i.e., the cleavage of $C_{\text{secondary}}$ – C_{primary} . The same group also observed that under higher hydrogen pressures, the yield of C15 from terminal dissociation was lower than the average of the internal dissociation product yields, which is similar to our result that only a low yield of C19 was obtained at 60 bar of H_2 . Notably, Nakagawa et al. found no significant difference between the yields of C2–C14 hydrocarbons, whereas we observed that the main products, C18 and C17, were acquired with the presence of a solvent.

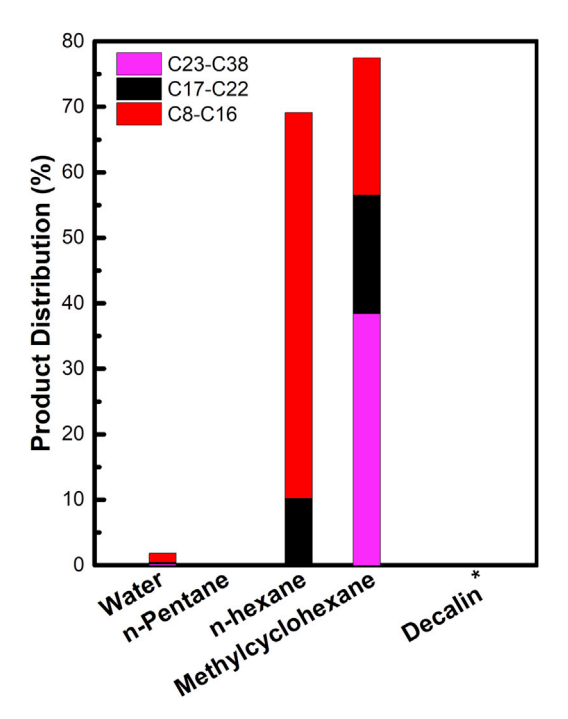
Likewise, HDPE is a linear alkane polymer containing predominantly secondary C atoms and a few primary C atoms; the influence of hydrogen pressure on the hydrogenolysis of HDPE seems similar to that of eicosane. At low $\rm H_2$ pressures, the liquid alkane products might mainly be generated from the terminal dissociation, which was suppressed with increasing $\rm H_2$ pressure. After the $\rm H_2$ pressure passed a threshold value, the internal dissociation became dominant. At 60 bar of $\rm H_2$, ~90% of HDPE was converted to C8+ liquid hydrocarbon products, implying that internal dissociation is the primary depolymerization pathway at high $\rm H_2$ pressures. However, both terminal and internal dissociation can coexist in a wide range of $\rm H_2$ pressures during HDPE depolymerization.

Solvent effect

Solute solubility and thermodynamic equilibrium coefficients are critical parameters that affect the reaction kinetics in solutions. 45 Here, the role of different organic solvents in HDPE depolymerization was investigated. In a polar solvent, e.g., water, the HDPE degradation rate was found to be very slow at 220° C, as shown in Figure 7.



Chem Catalysis Article



depolymerization of HDPE
Reaction conditions: 0.1 g HDPE,
25 mL solvent, 220°C, p(H₂) 20 bar,
1 h, 700 rpm. *In decalin, 5.4% of
HDPE was converted, but no
detectable liquid hydrocarbon
products were observed on GC-MS

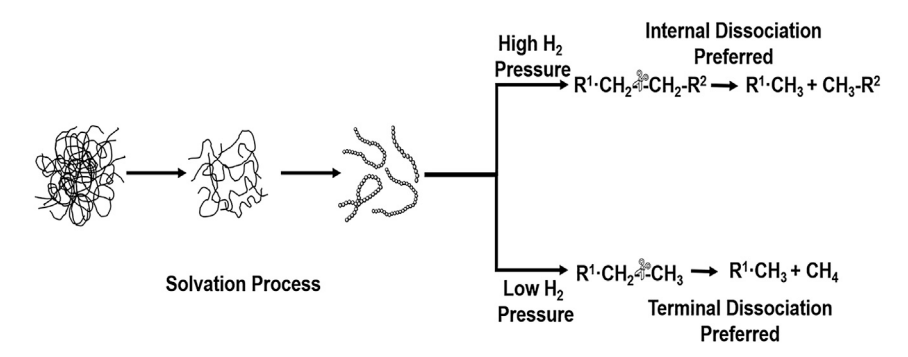
Figure 7. Solvent effect on

Typically, PE can be degraded in supercritical water whose dielectric constant is comparable to those of the polar organic solvents. 46,47 Although the supercritical hydrolysis process requires a very high energy input, the low polarity of supercritical water facilitates PE's dissolubility and thus promotes the reaction rate. However, at 220°C, subcritical water is much denser and more polar than supercritical water, leading to a low PE solubility and thus a slow depolymerization reaction rate. Meanwhile, we observed that the HDPE strips were transformed into spherical solid particles after the reaction, which was different from that in the organic solvents (Figure S2). These plastic strips usually melted at over 150°C. 48 The formation of spherical solids indicated that the plastic strips were melted but were not solvated in the water at 220°C as a result of the low-solubility HDPE in subcritical water. Therefore, non-polar solvents were preferred for PE dissolution and depolymerization. Figure 7 shows that *n*-hexane was the optimal organic solvent for HDPE degradation with the Ru/C catalyst, whereas other non-polar solvents exhibited much different performance in the depolymerization reaction. Notably, no cracking products were detected in *n*-pentane solvent, although the polarity of *n*-pentane is very similar to that of n-hexane. Here, the reaction temperature (220°C) was higher than n-pentane's critical temperature (196.45°C) but lower than n-hexane's critical temperature (234.5°C). Therefore, the supercritical pentane solvent behaved very differently from those at lower temperatures. HDPE polymers might not be solvated in the supercritical n-pentane, causing high resistance to mass and heat transfer. We also observed that the HDPE strips were transformed into spherical particles in the supercritical n-pentane after the reaction, implying that HDPE was melted rather than dissolved.

We evaluated the solvation effect by using the Hansen solubility parameters, which are based on the theory of "like dissolves like." ⁴⁹ As shown in Tables S1 and S2, the relative energy difference (RED) of water and PE is much larger than 1, indicating that water is not a suitable solvent for PE. The RED values are less than 1 for other organic solvents that show a high affinity, consistent with the experimental results that HDPE

Article





Scheme 1. HDPE polymer degradation pathways in the solvent

polymer could be dissolved in these solvents. It is reasonable that PE solvation in the solvents is the first step in the degradation reaction (Scheme 1). We observed that the solvent molecular structure profoundly affects the depolymerization, as shown in Figure 7. For instance, methylcyclohexane was not as efficient as n-hexane for depolymerization because of its obstructive cyclic molecular structure. Under identical reaction conditions, the dominant products with the n-hexane solvent are the medium-chain n-alkanes (C8-C16), whereas the longer-chain n-alkanes (C17-C38) are the main products in methylcyclohexane. Nevertheless, the appropriate inhibition effect on the PE depolymerization in methylcyclohexane was desired for controlling the product distribution given that the long-chain hydrocarbons (C17–C38) are the target products, such as lubricants, with a higher profit margin than the mediumchain n-alkanes (C8-C16), which are jet-fuel components. A similar steric hindrance effect was also observed with decalin as the solvent, whereby no cracking liquid hydrocarbon products were detected after the reaction. The solvated polymer molecules in decalin might be obstructed from being in contact with the heterogeneous Ru/C catalyst surface. Note that the molecular size of n-hexane is 1.03 nm (length) \times 0.49 nm (width) \times 0.4 nm (height), which is much larger than methylcyclohexane (0.79 \times 0.73 \times 0.5 nm) and slightly longer than decalin (0.91 \times 0.72 \times 0.5 nm). 50-52 Nevertheless, the linear molecules, e.g., n-hexane, were more flexible, compensating for their bulky molecular size. 53,54 The similarity in shape between n-hexane and HDPE could facilitate the diffusion of large PE oligomer molecules in the solvent, which allows the access of bulky reactant substrates to the Ru/C catalyst surface. In addition, methylcyclohexane and decalin are known as the hydrogendonor solvents,⁵⁵ which can transfer hydrogen even in the H₂ atmosphere. The solvent-donated H* could quickly react with the polymer radicals, terminating the consecutive cracking reactions. 56-58

According to the results of the molecular dynamics (MD) simulations, PE adopts a compact conformation in pentane and hexane, with the lowest radius of gyration value (R_g), followed by water and methylcyclohexane, and finally it adopts an extended conformation in *trans*-decalin (Table S3). The extended conformation of PE in decalin can be attributed to the high degree of hydrophobicity of decalin solvent. A PE molecule is also hydrophobic in nature and thus prefers to be in hydrophobic solvents, resulting in the fully extended conformation of the PE molecule in hydrophobic solvents such as decalin. To understand the influence that the structure might have on dynamic properties, we computed the end-to-end polymer chain autocorrelation function in different solvents, as shown in Figure 8, which estimates how readily the polymer relaxes in a particular solvent.



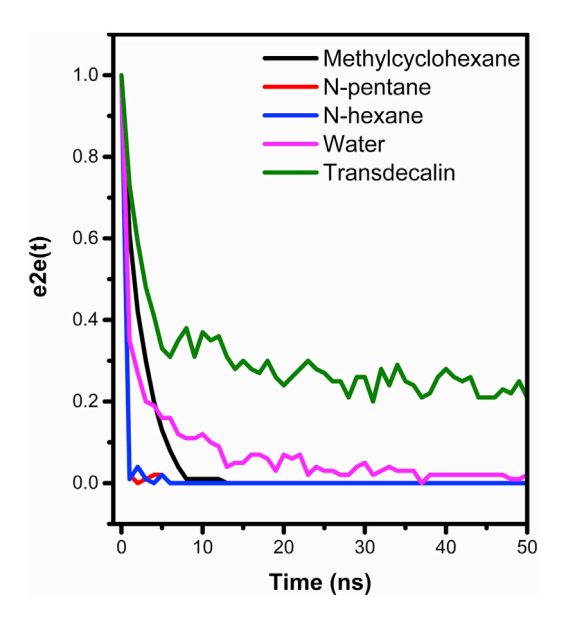


Figure 8. The autocorrelation function of end-to-end length of the polymer chain in different solvents

Figure 8 shows that PE polymer decorrelates fastest in *n*-pentane and *n*-hexane, followed by methylcyclohexane, water, and decalin. The decorrelation order of the PE polymer is in accordance with the amounts of short-chain hydrocarbon molecules produced in the experiment, except for *n*-pentane. In our simulations, PE decorrelated fastest in *n*-pentane; however, PE did not depolymerize in *n*-pentane to produce short-chain hydrocarbon molecules in the experiment. In this case, the difference observed between experiment and simulation is due to the limitation of simulations to capture supercritical behaviors of *n*-pentane. In our simulations at 493 K, *n*-pentane still behaved like a normal fluid rather than a supercritical one. As a result, the behavior of PE in *n*-pentane is similar to that in *n*-hexane.

The PE end-to-end length decorrelation rate correlates to the affinity of PE polymer toward the solvent it is immersed in, as described by the radius of gyration results. As the simulation progresses, the interaction between PE polymer and solvent molecules causes the conformation of the PE polymer to change. The cases in which the PE end-to-end length decorrelates fast (for example, in n-hexane) indicate that the PE polymer does not have a high affinity toward solvent molecules, thus causing the PE polymer to coil. We propose that the coiled polymer adsorbs in this state on the catalyst surface and undergoes cracking reactions. The coiled structure has a high tendency to pass through the solvent molecules to reach the catalyst surface. In contrast, the slow decorrelation rate of PE in decalin shows PE affinity toward decalin, where PE polymer can sustain extended conformations for a longer time. The comparison between PE conformation in decalin and in hexane after 500 ns of NVT (substance, volume, and temperature) simulations is shown in Figure 9. The straight PE chain in decalin has a high affinity toward solvent molecules, preventing the straight PE chain from reaching the catalyst surface for depolymerization reactions and leading to poor kinetic performance. The extended configurations of PE in decalin suggest higher relative thermodynamic stability in the bulk solvent as a result of increased entropy arising from the chain flexibility in the solvent. This result suggests that considering both the solvent quality and the adsorption affinity of collapsed and extended PE chains could

Article



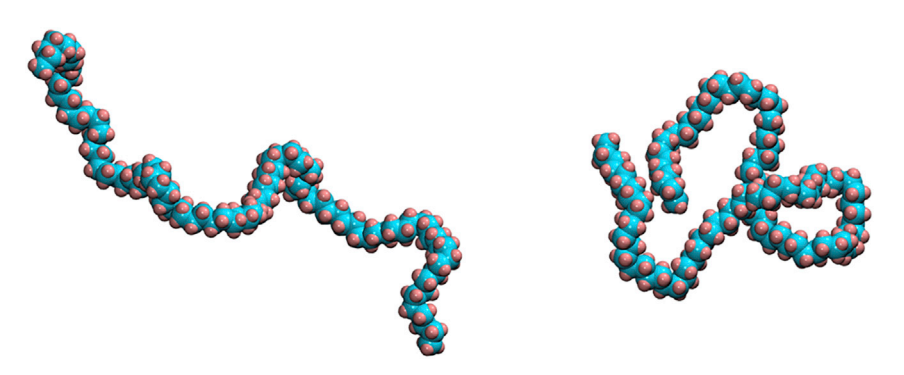


Figure 9. PE conformation in decalin (left) and in hexane (right) after 500 ns NVT simulations

determine an additional important screening characteristic for solvents used in depolymerization processes.

Stability

The catalyst stability is a big hurdle in plastic depolymerization via catalytic pyrolysis.^{59,60} In our study, the catalyst did not show severe deactivation in the n-hexane solvent after being used for five cycles (Figure 10). The yield of jet-fuelrange alkanes (C8-C16) decreased only slightly after first use and then became stable in the subsequent runs, indicating that the catalyst stability would be reliable for depolymerization. We observed that more short-chain hydrocarbons were generated after the first cycle, which could be ascribed to the increase in Ru particle size. Nakagawa et al. found that the terminal dissociation was more prevalent if the Ru particle size increased from <1.5 to >2 nm. 44 Therefore, smaller particle size might favor the yield of jet-fuel-range products. Furthermore, the thermal gravimetric analysis (TGA) curves showed that the Ru loading decreased by 0.62% after the first cycle and remained almost the same after the second cycle (Figure S3), which is consistent with the trend of decrease in the metallic surface area in Table 1. Both results demonstrated that Ru would not continuously leach after the first use.

Because of the high catalytic activity of the Ru catalyst in cleavage of the C-C bond, the solvent stability is important for the PE hydrogenolysis process. A blank experiment was conducted without the addition of HDPE (0.05 g Ru/C, 25 mL n-hexane, 220°C, p(H₂) 20 bar, 1 h, 700 rpm). Approximately 5.6 wt % of the solvent (including 5.1 wt % loss by evaporation) was lost after the reaction, which was much lower than in the cross-alkane metathesis process for PE depolymerization (15.1 wt % loss) with light alkanes as both the solvent and the feedstock and (t-Bu₂PO-^{t-Bu}POCOP) $Ir(C_2H_4)/\gamma$ -Al₂O₃ and Re₂O₇/ γ -Al₂O₃ as catalysts at 175°C for 4 days.²⁹ Moreover, for process optimization, the short-chain hydrocarbon products from HDPE depolymerization could be reused as the makeup solvent in the process.

DISCUSSION

In summary, we have demonstrated an efficient liquid-phase hydrogenolysis process with the heterogeneous Ru/C catalyst for selective depolymerization of waste HDPE plastic under mild conditions. Approximately 90 wt % HDPE was converted to C8+ liquid hydrocarbon products in an n-hexane solvent within 1 h under 30 bar H₂ at 220°C. We were able to tune the product distribution by adjusting the process conditions, including catalyst loading, reaction temperature, hydrogen pressure, and reaction time. With high catalyst loading, high reaction temperature, or prolonged reaction time, excess cracking occurred during the reaction and led to the



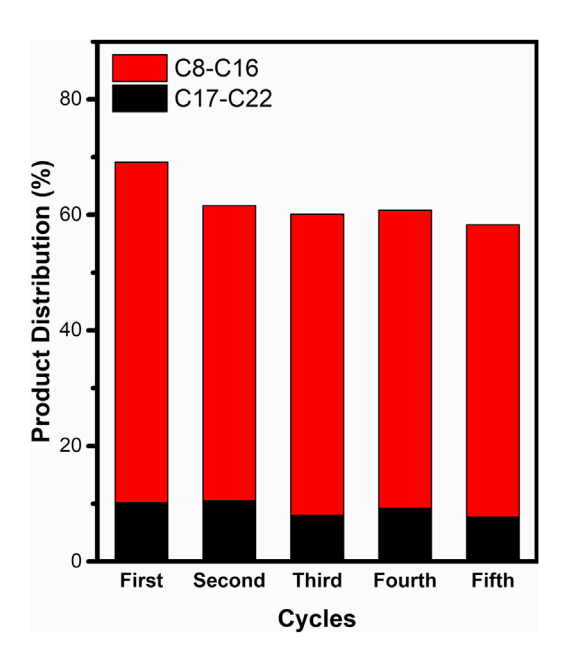


Figure 10. Lifetime of the catalyst Reaction conditions: 0.1 g HDPE, 0.05 g Ru/C, 25 mL *n*-hexane, 220°C, p(H₂) 20 bar, 1 h, 700 rpm. The excess is light hydrocarbons (C1–C7).

production of less valuable short-chain hydrocarbons. Hydrogen pressure played a significant role in the polymer dissociation pathway. Under low H_2 pressures, terminal dissociation was dominant, whereas internal dissociation was prevalent when the H_2 pressure increased.

Furthermore, solvents also profoundly affected the depolymerization reaction kinetics and product selectivity. The solvation ability of PE in solvents was a key factor for depolymerization. The degradation of HDPE in subcritical water was slow because of its low solubility in polar solvents. Among the non-polar hydrocarbon solvents, *n*-hexane (a linear alkane) was better for HDPE depolymerization than the cyclic alkanes (methylcyclohexane and decalin). The highest yield of jet-fuel-range hydrocarbons (C8–C16) reached 60.8 wt % in the *n*-hexane solvent at 220°C. The MD simulations suggest that the interaction between PE polymers and solvent molecules causes the conformation of the PE polymer to change. The PE polymer with a low affinity toward solvent molecules tends to coil and then sieve through solvent molecules and get to the catalyst surface, where it will get cracked. PE adopts a compact coil conformation in pentane and hexane, followed by water, methylcyclohexane, and decalin. Although the steric hindrance from the solvents' cyclic molecular structure inhibited PE depolymerization, it promoted the production of long-chain hydrocarbons, such as lubricants.

EXPERIMENTAL PROCEDURES

Resource availability

Lead contact

Further information and requests for resources should be directed to and will be fulfilled by the lead contact, Hongfei Lin (hongfei.lin@wsu.edu).

Materials availability

This study did not generate any new unique reagent or material.

Data and code availability

This study did not generate codes, software, or algorithms.

Article



Materials

The feedstocks, HDPE plastic water jugs, were collected from the local recycling center in Pullman, Washington. Before the experiment, the jugs were cleaned with deionized water, dried at 100° C, and then cut into strips (5 × 5 mm). All chemicals were used as received without further treatment. The catalysts (Ru/C [5% Ru basis], Pd/C [5% Pd basis], Pt/C [5% Pt basis], and Rh/C [5% Rh basis]), the catalyst precursors (copper(II) nitrate trihydrate [99%] and iron(III) nitrate nonahydrate [98%]), and the self-synthesized catalyst support (activated charcoal Norit) were supplied from Sigma-Aldrich. Nickel(II) nitrate hexahydrate (99%) was purchased from Millipore Sigma. p-xylene (99%) was purchased from Alfa Aesar. Ultrapure water (specific resistance of 18.2 M Ω cm⁻¹), n-pentane (Alfa Aesar, 98%), n-hexane (J.T. Baker, 95%), methylcyclohexane (Alfa Aesar, 99%), and decalin (Tokyo Chemical Industry, 99%) were used as the solvents.

5% Cu/C, 5% Fe/C, and 5% Ni/C were synthesized through impregnation with copper nitrate trihydrate, iron nitrate nonahydrate, and nickel nitrate hexahydrate, respectively, as the metal precursors and activated charcoal Norit as the support. After being dried, the as-prepared 5% Ni/C, 5% Fe/C, and 5% Ni/C samples were calcined at 350°C (Ni/C) or 500°C (Fe/C and Ni/C) for 3 h in an atmosphere of nitrogen. Finally, the catalysts were reduced in H_2 flow at 400°C (Ni/C) or 500°C (Fe/C and Ni/C) for 5 h prior to use.

Characterization

The specific surface area of the catalysts was determined through single-point adsorption of N₂ at 77 K with a Micromeritics Autochem II 2920. The samples were prepared in helium at 200°C for 1 h before nitrogen adsorption (30% N_2 /He).

The CO pulse chemisorption was used for determining the metal dispersion, activemetal particle size, and metallic surface area. The test was carried out on a Micromeritics Autochem II 2920. The sample was reduced for 2 h at 300°C with 10% H₂/Ar at a 50 mL/min flow rate and then purged with helium for 1 h at a flow rate of 50 mL/min. After the sample was cooled to ambient temperature, 10% CO/He was added at each pulse, and the CO uptake profile was measured with a thermal conductivity detector (TCD) until no CO was adsorbed. The Ru dispersion was calculated under the assumption of a CO/Ru stoichiometry of 1:1.61

The fresh and spent Ru/C catalysts were characterized by TEM on a JEOL 2010 J microscope at an accelerating voltage of 200 kV. The Gatan Digital Micrograph software was used for conducting data processing and analysis. The catalyst powder samples were dispersed on Formvar film nickel grids (200 mesh).

The XPS analyses were carried out on a Kratos AXIS-165 with a monochromatized Al-K α X-ray anode (1,486.6 eV) with the C 1s peak at 284.6 eV as the internal reference. The deconvolutions of Ru 3p were analyzed with the software XPSPEAK version 4.1.

The crystalline catalyst structure was evaluated by X-ray powder diffraction (Rigaku Miniflex 600), with a Co-K α radiation source ($\lambda = \mathring{A}$) at a 2 θ step of 10 $^{\circ}$ -90 $^{\circ}$ with a step size of 0.02° .

TGA was performed with a TA Instruments Q50. The samples were loaded in aluminum crucibles and heated in airflow (60 mL/min) from 25°C to 600°C at a heating rate of 10°C/min.



Reaction procedure

The depolymerization experiments were carried out in a 45 mL elevated pressure and temperature Parr Series 5000 multiple reactor system with a 4871 temperature controller. In a typical experiment, a certain amount of HDPE strips and catalyst were loaded in 25 mL solvent. The vessels were sealed and purged five times with 400 psi N_2 and three times with 400 psi N_2 and then pressurized with N_2 to the set pressure at ambient temperature. Then the reactor was heated up to the set reaction temperature with magnetic stirring at 700 rpm. After the reaction, the vessel was quenched in a cold bath for fast cooling.

Analysis

After the reaction, the reactor was connected to a gas chromatograph Shimadzu GC-2014 with a TCD for analysis of the gas-phase product samples. The columns included a right 12.5 m (I) \times 0.32 mm (i.d.) packed column, which comprised 3 m Hayesep D, 4 m HS, and 2.5 m HN, and a left 2 m (I) \times 0.32 mm (i.d.) 10% Carbowax 20 m Ch packed column. After the reactor was disassembled, the solid catalyst and non-dissolvable residues were filtered out of the liquid phase. Then the liquid product samples were collected, and the internal standard, *p*-xylene, was added. The liquid samples were analyzed by a QP-2020 (Shimadzu) gas chromatograph-mass spectrometer for identifying and quantifying the unknown products. The QP-2020 was equipped with a Shimadzu SH-Rxi-5SIL MS column (30 m \times 0.25 mm i.d., 0.25 μ m film thickness), a flame ionization detector, and a high-performance ion source. The following definitions were used for quantitating the weight yield (y):

$$y = \frac{\sum m_x}{m_0} \times 100 \%,$$

where m_0 is the weight of the HDPE feedstock before reaction and m_x is the weight of the alkane hydrocarbons after the reaction, where x means the C number.

MD simulations

A PE molecule $C_{100}H_{202}$ in length was packed into five different simulation boxes of $10 \times 10 \times 10 \text{ nm}^3$. Each box was filled with one of the five different solvents: methylcyclohexane, n-pentane, n-hexane, water, or decalin. Water was modeled with the SPC/E water force field, 62 while the force fields for the organic solvents were obtained from the Automated Topology Builder repository. 63 For decalin, the isomer used was trans-decalin because trans-decalin is more stable than its cis counterpart as a result of its diequatorial chair conformation. Each system was simulated with the GROMACS 2018.3 simulation package.⁶⁴ The steepest descent algorithms were used for removing unfavorable contacts in the initial configuration. Electrostatic interactions were calculated with the particle mesh Ewald summation method⁶⁵ with an electrostatic cutoff value of 1.0 nm and van der Waals cutoff value of 1.0 nm. The system was evolved in the NPT ensemble (temperature 493 K, pressure 1 atm) for 2 ns with the Donadio-Bussi-Parrinello thermostat⁶⁶ (time constant $\tau = 0.1$ ps) and the Berendsen barostat⁶⁷ (time constant τ = 1 ps). A temperature of 493 K was chosen to be consistent with the experiment. All the dimensions of the box were allowed to change during the NPT simulation. The production runs were carried out in the NVT ensemble (temperature 493 K), where the temperature was maintained by the Donadio-Bussi-Parrinello thermostat (time constant $\tau = 0.1$ ps) for 500 ns.

The polymer structure in the solvent was captured through the average radius of gyration calculated over the entire simulation time of 500 ns. To assess the dynamic



behavior of the polymer in different solvents, we calculated the end-to-end autocorrelation function according to the following equation:

e2e(t)
$$\equiv \frac{\langle \mathbf{A}(t) \cdot \mathbf{A}(0) \rangle}{\langle \mathbf{A}(0) \cdot \mathbf{A}(0) \rangle}$$

where A is the vector from the first C atom to the last C atom along the polymer chain.

SUPPLEMENTAL INFORMATION

Supplemental information can be found online at https://doi.org/10.1016/j.checat. 2021.04.002.

ACKNOWLEDGMENTS

This project was partially funded by the Washington State University internal fund and Washington Research Foundation. C.J. is thankful for the Chambroad Fellowship from the Gene and Linda Voiland School of Chemical Engineering and Bioengineering at Washington State University. Computational simulation in this research was supported by NSF-CBET award 1703638 and was facilitated through the use of advanced computational, storage, and networking infrastructure provided by the Hyak supercomputer system at the University of Washington. The authors would like to acknowledge Zengran Sun and Prof. Steven R. Saunders for their support in the thermal gravimetric analysis. The authors also thank Dr. Baoming Zhao and Prof. Jinwen Zhang for valuable discussions.

AUTHOR CONTRIBUTIONS

H.L. proposed, designed, and guided the project and revised the manuscript. C.J. performed most of the experiments and drafted the manuscript. S.X. and W.Z. also took part in the experiments and revised the manuscript. N.I., J.S., and J.P. performed the molecular dynamics simulations. All authors checked the manuscript.

DECLARATION OF INTERESTS

The authors declare no competing interests.

Received: December 18, 2020 Revised: March 14, 2021 Accepted: April 7, 2021 Published: May 17, 2021

REFERENCES

- 1. Jambeck, J.R., Geyer, R., Wilcox, C., Siegler, T.R., Perryman, M., Andrady, A., Narayan, R., and Law, K.L. (2015). Plastic waste inputs from land into the ocean. Science 347, 768-771.
- 2. Law, K.L., Starr, N., Siegler, T.R., Jambeck, J.R., Mallos, N.J., and Leonard, G.H. (2020). The United States' contribution of plastic waste to land and ocean. Sci. Adv. 6, eabd0288.
- 3. Ostle, C., Thompson, R.C., Broughton, D., Gregory, L., Wootton, M., and Johns, D.G. (2019). The rise in ocean plastics evidenced from a 60-year time series. Nat. Commun. 10,
- 4. Geyer, R., Jambeck, J.R., and Law, K.L. (2017). Production, use, and fate of all plastics ever made. Sci. Adv. 3, e1700782.

- 5. Rosevelt, C., Los Huertos, M., Garza, C., and Nevins, H.M. (2013). Marine debris in central California: quantifying type and abundance of beach litter in Monterey Bay, CA. Mar. Pollut. Bull. 71, 299-306.
- 6. Al-Salem, S.M., Lettieri, P., and Baeyens, J. (2009). Recycling and recovery routes of plastic solid waste (PSW): a review. Waste Manag. 29, 2625-2643
- 7. Rahimi, A.R., and Garciá, J.M. (2017). Chemical recycling of waste plastics for new materials production. Nat. Rev. Chem. 1, 0046.
- 8. Chevron Phillips Chemical. (2020). Chevron Phillips Chemical successfully completes first U.S. commercial scale production of circular polyethylene from recycled mixed-waste

- plastics, https://www.cpchem.com/mediaevents/news/press-release/chevron-phillipschemical-successfully-completes-first-us.
- 9. SABIC. (2020). SABIC outlines intentions for TrucircleTM to close loop on plastic recycling. https://www.sabic.com/en/news/21891-sabic outlines-intentions-for-trucircle-to-close-loopon-plastic-recycling.
- 10. BASF (2018). ChemCycling $^{\text{TM}}$: turning plastic waste into new chemical products. https:// www.basf.com/global/en/who-we-are/ sustainability/we-drive-sustainable-solutions/ circular-economy/mass-balance-approach/ chemcycling.html.
- 11. Kaimal, V.K., and Vijayabalan, P. (2016). A study on synthesis of energy fuel from waste plastic



- and assessment of its potential as an alternative fuel for diesel engines. Waste Manag. 51, 91–96.
- Marcilla, A., Beltrán, M.I., and Navarro, R. (2009). Thermal and catalytic pyrolysis of polyethylene over HZSM5 and HUSY zeolites in a batch reactor under dynamic conditions. Appl. Catal. B Environ. 86, 78–86.
- Kunwar, B., Moser, B.R., Chandrasekaran, S.R., Rajagopalan, N., and Sharma, B.K. (2016). Catalytic and thermal depolymerization of low value post-consumer high density polyethylene plastic. Energy 111, 884–892.
- Zhang, Y., Duan, D., Lei, H., Villota, E., and Ruan, R. (2019). Jet fuel production from waste plastics via catalytic pyrolysis with activated carbons. Appl. Energy 251, 113337.
- Kaminsky, W., and Zorriqueta, I.J.N. (2007).
 Catalytical and thermal pyrolysis of polyolefins.
 J. Anal. Appl. Pyrolysis 79, 368–374.
- Das, P., and Tiwari, P. (2018). Valorization of packaging plastic waste by slow pyrolysis. Resour. Conserv. Recycl. 128, 69–77.
- Park, K.B., Jeong, Y.S., Guzelciftci, B., and Kim, J.S. (2019). Characteristics of a new type continuous two-stage pyrolysis of waste polyethylene. Energy 166, 343–351.
- Castaño, P., Elordi, G., Olazar, M., Aguayo, A.T., Pawelec, B., and Bilbao, J. (2011). Insights into the coke deposited on HZSM-5, Hβ and HY zeolites during the cracking of polyethylene. Appl. Catal. B Environ. 104, 91–100.
- Marcilla, A., Gómez-Siurana, A., and Valdés, F.J. (2008). Influence of the temperature on the composition of the coke obtained in the catalytic cracking of low density polyethylene in the presence of USY and HZSM-5 zeolites. Microporous Mesoporous Mater. 109, 420-428.
- Lin, Y.H., and Yang, M.H. (2005). Catalytic reactions of post-consumer polymer waste over fluidised cracking catalysts for producing hydrocarbons. J. Mol. Catal. A. Chem. 231, 113–122.
- Ibáñez, M., Artetxe, M., Lopez, G., Elordi, G., Bilbao, J., Olazar, M., and Castaño, P. (2014). Identification of the coke deposited on an HZSM-5 zeolite catalyst during the sequenced pyrolysis-cracking of HDPE. Appl. Catal. B Environ. 148–149, 436–445.
- 22. Dufaud, V., and Basset, J.M. (1998). Catalytic hydrogenolysis at low temperature and pressure of polyethylene and polypropylene to diesels or lower alkanes by a zirconium hydride supported on silica-alumina: a step toward polyolefin degradation by the microscopic reverse of Ziegler-Natta pol. Angew. Chem. Int. Ed. 37, 806–810.
- 23. Tennakoon, A., Wu, X., Paterson, A.L., Patnaik, S., Pei, Y., LaPointe, A.M., Ammal, S.C., Hackler, R.A., Heyden, A., Slowing, I.I., et al. (2020). Catalytic upcycling of high-density polyethylene via a processive mechanism. Nat. Catal. *3*, 893–901.
- Zhang, F., Zeng, M., Yappert, R.D., Sun, J., Lee, Y.H., LaPointe, A.M., Peters, B., Abu-Omar, M.M., and Scott, S.L. (2020). Polyethylene upcycling to long-chain alkylaromatics by

- tandem hydrogenolysis/aromatization. Science *370*, 437–441.
- Vicente, G., Aguado, J., Serrano, D.P., and Sánchez, N. (2009). HDPE chemical recycling promoted by phenol solvent. J. Anal. Appl. Pyrolysis 85, 366–371.
- Serrano, D.P., Aguado, J., Vicente, G., and Sánchez, N. (2007). Effects of hydrogendonating solvents on the thermal degradation of HDPE. J. Anal. Appl. Pyrolysis 78, 194–199.
- Aguado, J., Serrano, D.P., Vicente, G., and Sánchez, N. (2007). Enhanced production of α-olefins by thermal degradation of High-Density Polyethylene (HDPE) in decalin solvent: effect of the reaction time and temperature. Ind. Eng. Chem. Res. 46, 3497–3504.
- Adams, C.J., Earle, M.J., and Seddon, K.R. (2000). Catalytic cracking reactions of polyethylene to light alkanes: in ionic liquids. Green. Chem. 2, 21–23.
- Jia, X., Qin, C., Friedberger, T., Guan, Z., and Huang, Z. (2016). Efficient and selective degradation of polyethylenes into liquid fuels and waxes under mild conditions. Sci. Adv. 2, e1501591.
- Zhang, J., Huo, X., Li, Y., and Strathmann, T.J. (2019). Catalytic hydrothermal decarboxylation and cracking of fatty acids and lipids over Ru/C. ACS Sustain. Chem. Eng. 7, 14400–14410.
- Oya, S.I., Kanno, D., Watanabe, H., Tamura, M., Nakagawa, Y., and Tomishige, K. (2015).
 Catalytic production of branched small alkanes from biohydrocarbons. ChemSusChem 8, 2472–2475.
- Sinfelt, J.H. (1973). Specificity in catalytic hydrogenolysis by metals. Adv. Catal. 23, 91–119.
- 33. Rorrer, J.E., Beckham, G.T., and Román-Leshkov, Y. (2021). Conversion of polyolefin waste to liquid alkanes with Ru-based catalysts under mild conditions. JACS Au 1, 8–12.
- Li, Y., Ma, L., Liu, H., and He, D. (2014). Influence of HZSM5 on the activity of Ru catalysts and product selectivity during the hydrogenolysis of glycerol. Appl. Catal. A. Gen. 469, 45–51.
- Ding, W.B., Tuntawiroon, W., Liang, J., and Anderson, L.L. (1996). Depolymerization of waste plastics with coal over metal-loaded silica - alumina catalysts. Fuel Process. Technol. 49, 49–63.
- Celik, G., Kennedy, R.M., Hackler, R.A., Ferrandon, M., Tennakoon, A., Patnaik, S., Lapointe, A.M., Ammal, S.C., Heyden, A., Perras, F.A., et al. (2019). Upcycling single-use polyethylene into high-quality liquid products. ACS Cent. Sci. 5, 1795–1803.
- Coq, B., Dutartre, R., Figueras, F., and Tazi, T. (1990). Particle size, precursor, and support effects in the hydrogenolysis of alkanes over supported rhodium catalysts. J. Catal. 122, 438–447.
- Akubo, K., Nahil, M.A., and Williams, P.T. (2019). Aromatic fuel oils produced from the pyrolysis-catalysis of polyethylene plastic with metal-impregnated zeolite catalysts. J. Energy Inst. 92, 195–202.

- Almithn, A., and Hibbitts, D. (2019). Comparing rate and mechanism of ethane hydrogenolysis on transition-metal catalysts. J. Phys. Chem. C 123, 5421–5432.
- Flaherty, D.W., Hibbitts, D.D., and Iglesia, E. (2014). Metal-catalyzed C-C bond cleavage in alkanes: effects of methyl substitution on transition-state structures and stability. J. Am. Chem. Soc. 136, 9664–9676.
- Flaherty, D.W., Hibbitts, D.D., Gürbüz, E.I., and Iglesia, E. (2014). Theoretical and kinetic assessment of the mechanism of ethane hydrogenolysis on metal surfaces saturated with chemisorbed hydrogen. J. Catal. 311, 350–356.
- Hibbitts, D.D., Flaherty, D.W., and Iglesia, E. (2016). Effects of chain length on the mechanism and rates of metal-catalyzed hydrogenolysis of n-alkanes. J. Phys. Chem. C 120, 8125–8138.
- Flaherty, D.W., and Iglesia, E. (2013). Transition-state enthalpy and entropy effects on reactivity and selectivity in hydrogenolysis of n -alkanes. J. Am. Chem. Soc. 135, 18586– 18599.
- Nakagawa, Y., Oya, S., Kanno, D., Nakaji, Y., Tamura, M., and Tomishige, K. (2017).
 Regioselectivity and reaction mechanism of Rucatalyzed hydrogenolysis of squalane and model alkanes. ChemSusChem 10, 189–198.
- Shuai, L., and Luterbacher, J. (2016). Organic solvent effects in biomass conversion reactions. ChemSusChem 9, 133–155.
- Moriya, T., and Enomoto, H. (1999). Characteristics of polyethylene cracking in supercritical water compared to thermal cracking. Polym. Degrad. Stab. 65, 373–386.
- Su, X., Zhao, Y., Zhang, R., and Bi, J. (2004). Investigation on degradation of polyethylene to oils in supercritical water. Fuel Process. Technol. 85, 1249–1258.
- Park, J.W., Kim, J.H., and Seo, G. (2002). The effect of pore shape on the catalytic performance of zeolites in the liquid-phase degradation of HDPE. Polym. Degrad. Stab. 76, 495–501.
- 49. Hansen, C.M. (2007). Hansen Solubility Parameters: A User's Handbook, Second edition (CRC Press).
- Barrer, R.M., and Sikand, A. (1979). Sorption of hydrocarbons and water in silanated and unsilanated partial H-forms of zeolite Y. J. Chem. Soc. Faraday Trans. 1 Phys. Chem. Condens. Phases 75, 2221–2234.
- Drozdowski, H., and Nowakowski, K. (2008). Xray diffraction studies of liquid methylcyclohexane C6Hn- CH3 structure at 293 K. Acta Phys. Pol. A 114, 383–389.
- Cardenal, A.D., Jeong Park, H., Chalker, C.J., Ortiz, K.G., and Powers, D.C. (2017). Cis

 Decalin oxidation as a stereochemical probe of in-MOF versus on-MOF catalysis. Chem. Commun. 53, 7377–7380.
- Park, G.S., and Saleem, M. (1984). Diffusion of additives and plasticizers in poly(vinyl chloride) - v. diffusion of n-hexadecane and ddt in various poly(vinyl chloride)/dialkylphthalate compositions. J. Memb. Sci. 18, 177–185.

Article

CellPress

- 54. Saleem, M., Asfour, A.A., De Kee, D., and Harrison, B. (1989). Diffusion of organic penetrants through low density polyethylene (LDPE) films: effect of size and shape of the penetrant molecules. J. Appl. Polym. Sci. 37,
- 55. Okada, Y., Sasaki, E., Watanabe, E., Hyodo, S., and Nishijima, H. (2006). Development of dehydrogenation catalyst for hydrogen generation in organic chemical hydride method. Int. J. Hydrogen Energy 31, 1348-1356.
- 56. Fujimoto, K., Ohno, A., and Kunugi, T. (1983). Liquid phase hydrogenolysis of thiophene by decaline as hydrogen donor with metal supported active carbon catalysts. Stud. Surf. Sci. Catal. 17, 241–249.
- 57. Chang, H.Z., Li, J.Q., Du, S., Shen, K.Y., Yang, Q., Yi, H., and Zhang, J.W. (2019). Transformation characteristics of hydrogendonor solvent tetralin in the process of direct coal liquefaction. Front. Chem. 7. https://doi. org/10.3389/fchem.2019.00737.

- 58. Sato, S., Murakata, T., Baba, S., Saito, Y., and Watanabe, S. (1990). Solvent effect on thermal degradation of polystyrene. J. Appl. Polym. Sci. 40, 2065-2071.
- 59. Renzini, M.S., Lerici, L.C., Sedran, U., and Pierella, L.B. (2011). Stability of ZSM-11 and BETA zeolites during the catalytic cracking of low-density polyethylene. J. Anal. Appl. Pyrolysis 92, 450-455.
- 60. Barbarias, I., Artetxe, M., Lopez, G., Arregi, A., Bilbao, J., and Olazar, M. (2018). Influence of the conditions for reforming HDPE pyrolysis volatiles on the catalyst deactivation by coke. Fuel Process. Technol. 171, 100-109.
- 61. Zhang, H., Li, W., Jin, Y., Sheng, W., Hu, M., Wang, X., and Zhang, J. (2016). Ru-Co(III)-Cu(II)/SAC catalyst for acetylene hydrochlorination. Appl. Catal. B Environ. 189,
- 62. Perera, L., and Berkowitz, M.L. (1991). Manybody effects in molecular dynamics simulations of Na +(H2O)n and Cl-(H2O) n clusters. J. Chem. Phys. 95, 1954-1963.

- 63. Malde, A.K., Zuo, L., Breeze, M., Stroet, M., Poger, D., Nair, P.C., Oostenbrink, C., and Mark, A.E. (2011). An automated force field Topology builder (ATB) and repository: version 1.0. J. Chem. Theor. Comput. 7, 4026-4037.
- 64. Abraham, M.J., Murtola, T., Schulz, R., Páll, S., Smith, J.C., Hess, B., and Lindah, E. (2015). Gromacs: high performance molecular simulations through multi-level parallelism from laptops to supercomputers. SoftwareX 1-*2*, 19–25.
- 65. Darden, T., York, D., and Pedersen, L. (1993). Particle mesh Ewald: an $N \cdot \log(N)$ method for Ewald sums in large systems. J. Chem. Phys. 98, 10089-10092.
- 66. Bussi, G., Donadio, D., and Parrinello, M. (2007). Canonical sampling through velocity rescaling. J. Chem. Phys. 126, 014101.
- 67. Berendsen, H.J.C., Postma, J.P.M., van Gunsteren, W.F., DiNola, A., and Haak, J.R. (1984). Molecular dynamics with coupling to an external bath. J. Chem. Phys. 81, 3684-3690.